# Tricyclic antidepressants inhibit hippocampal α7* and α9α10 nicotinic acetylcholine receptors by different mechanisms

Hugo R. Arias[a],*, Elizabeth Vázquez-Gómez[b], Andy Hernández-Abrego[b], Sofía Gallino[c], Dominik Feuerbach[d], Marcelo O. Ortells[e], Ana Belén Elgoyhen[c,f], Jesús García-Colunga[b]

[a] Department of Basic Sciences, California Northstate University College of Medicine, Elk Grove, CA, USA
[b] Departamento de Neurobiología Celular y Molecular, Instituto de Neurobiología, Universidad Nacional Autónoma de México, Querétaro, Mexico
[c] Instituto de Investigaciones en Ingeniería Genética y Biología Molecular, Dr. Héctor N. Torres, CONICET, Facultad de Medicina, Universidad de Buenos Aires, Argentina
[d] Novartis Institutes for Biomedical Research, Basel, Switzerland
[e] Facultad de Medicina, Universidad de Morón, Morón, CONICET, Argentina
[f] Instituto de Farmacología, Facultad de Medicina, Universidad de Buenos Aires, Argentina

ARTICLE INFO

ABSTRACT

The activity of tricyclic antidepressants (TCAs) at α7 and α9α10 nicotinic acetylcholine receptors (AChRs) as well as at hippocampal α7-containing (i.e., α7*) AChRs is determined by using $Ca^{2+}$ influx and electrophysiological recordings. To determine the inhibitory mechanisms, additional functional tests and molecular docking experiments are performed. The results established that TCAs (a) inhibit $Ca^{2+}$ influx in GH3-α7 cells with the following potency ($IC_{50}$ in μM) rank: amitriptyline (2.7 ± 0.3) > doxepin (5.9 ± 1.1) ~ imipramine (6.6 ± 1.0). Interestingly, imipramine inhibits hippocampal α7* AChRs (42.2 ± 8.5 μM) in a noncompetitive and voltage-dependent manner, whereas it inhibits α9α10 AChRs (0.53 ± 0.05 μM) in a competitive and voltage-independent manner, and (b) inhibit [$^3$H]imipramine binding to resting α7 AChRs with the following affinity rank ($IC_{50}$ in μM): imipramine (1.6 ± 0.2) > amitriptyline (2.4 ± 0.3) > doxepin (4.9 ± 0.6), whereas imipramine's affinity was no significantly different for that for the desensitized state. The molecular docking and functional results support the notion that imipramine noncompetitively inhibits α7 AChRs by interacting with two overlapping luminal sites, whereas it competitively inhibits α9α10 AChRs by interacting with the orthosteric sites. Collectively our data indicate that TCAs inhibit α7, α9α10, and hippocampal α7* AChRs at clinically relevant concentrations and by different mechanisms of action.

## 1. Introduction

The evidence showing a higher rate of smokers in depressed patients than in the general population supports the involvement of nicotinic acetylcholine receptors (AChRs) in depressive disorders (Mineur and Picciotto, 2010). In addition, chronic stress not only declines cognition in rodents but also increases the sensitivity of hippocampal neurons to cholinergic neurotransmission (Mizoguchi et al., 2001). This effect fits very well with the hypercholinergic hypothesis of depression, stating that an increased sensitivity of the cholinergic system over the noradrenergic system may develop in depressed mood states (Shytle et al., 2002; Mineur and Picciotto, 2010; Arias et al., 2014). In this regard, it is hypothesized that the therapeutic action of many antidepressants might

be mediated, at least partially, through inhibition of excessive neuronal AChR activity.

Alpha7-containing AChRs (i.e., α7* AChRs) are widely expressed in the brain, including the hippocampus, where they play important roles in memory mechanisms and in Alzheimer's disease and schizophrenia (Wallace and Porter, 2011). Nevertheless, the role of hippocampal α7* AChRs in stress, depression, and anxiety, is less known. On the other hand, α9α10 AChRs are expressed in outer hair cells where they regulate the fine tuning and high sensitivity of the mammalian inner ear and the efferent medial olivocochlear-hair cell synapse (Elgoyhen and Katz, 2012; Goutman et al., 2015). There is a large body of evidence indicating that α9 and α10 subunits are expressed in peripheral tissues and cells, including adrenal and pituitary glands (Mohammadi et al.,

2017), bone marrow, skin, sperm, and several immune cells (St-Pierre et al., 2016; Peng et al., 2004; Grando, 2006; Kumar and Meizel, 2005), but consistently not in the brain (Morley et al., 2018), in spite of the fact that a recent paper has described that these subunits are expressed in the CNS (Lykhmus et al., 2017). Since neuropathic pain was prevented by decreasing the activity of α9α10 AChRs (by using either knockout mice or selective antagonists), it has been considered that this receptor subtype is involved in pain-related mechanisms (McIntosh et al., 2009; Romero et al., 2017). Although the role of α9α10 AChRs in depression has not been proved, the anti-inflammatory activity elicited by several α9α10 AChR antagonists (McIntosh et al., 2009; Romero et al., 2017) could be considered a first step on this direction, especially considering a direct correlation between depression and inflammation (Christmas et al., 2011).

Tricyclic antidepressants (TCAs), a class of structurally related compounds that have been widely used for the treatment of depressive and anxiety mood disorders, inhibit different AChR subtypes (Arias et al., 2010b, 2010c; Feuerbach et al., 2005; Gumilar et al., 2003; López-Valdés et al., 2002; López-Valdés and García-Colunga, 2001). However, the functional activity of TCAs at α7 and α9α10 AChRs and thus, their potential role in depression and pain has not been fully characterized. In this regard, a better understanding of the interaction of the most widely used TCAs (i.e., imipramine, amitriptyline, and doxepin) (Fig. 1) with the α7 and α9α10 AChR subtypes as well as with hippocampal α7* AChRs, may clarify possible roles for these receptors as targets for the therapeutic action of these antidepressants. To further characterize the molecular interactions of TCAs with these AChRs, additional voltage-dependence and functional competition experiments, radioligand competition binding assays with α7 AChRs in different conformational states, molecular docking and molecular dynamics studies at α7 and α9α10 AChRs were performed.

## 2. Material and methods

### 2.1. Materials

[$^3$H]Imipramine (47.5 Ci/mmol) was obtained from PerkinElmer Life Sciences Products, Inc. (Boston, MA, USA) and [$^3$H]methyllycaconitine (100 Ci/mmol) was purchased from American Radiolabeled Chemicals Inc. (Saint Louis, MO, USA), and stored in ethanol at −20 °C. (-)-Nicotine tartrate, ( ± )-epibatidine hydrochloride, imipramine hydrochloride, amitriptyline hydrochloride, doxepin hydrochloride, probenecid, polyethylenimine, acetylcholine chloride (ACh), choline chloride (Ch), bovine serum albumin (BSA), BAPTA-AM, and methyllycaconitine citrate hydrate (MLA) were purchased from Sigma Chemical Co. (St. Louis, MO, USA). Fluo-4 was purchased from Molecular Probes (Eugene, Oregon, USA). α-Bungarotoxin (α-BTx) was obtained from Invitrogen Co. (Carlsbad, CA,USA). Salts were of analytical grade.

### 2.2. Ca$^{2+}$ influx measurements in GH3-hα7 cells

Ca$^{2+}$ influx was determined as previously described (Arias et al., 2010a; Vázquez-Gómez et al., 2014). Briefly, $5 \times 10^4$ GH3-hα7 cells per well were seeded 72 h prior to the experiment on black 96-well plates (Costar, New York, USA) and incubated at 37 °C in a humidified atmosphere (5% CO$_2$/95% air). 16–24 h before the experiment, the medium was changed to 1% BSA in Hepes-buffered salt solution (HBSS) containing (in mM): 130 NaCl, 5.4 KCl, 2 CaCl$_2$, 0.8 MgSO$_4$, 0.9 NaH$_2$PO$_4$, 25 glucose, 20 Hepes, pH 7.4. On the day of the experiment, the medium was removed by flicking the plates and replaced with 100 μL HBSS/1% BSA containing 2 mM Fluo-4 in the presence of 2.5 mM probenecid. The cells were then incubated at 37 °C in a humidified atmosphere (5% CO$_2$/95% air) for 1 h. Plates were flicked to remove excess of Fluo-4, washed twice with HBSS/1% BSA, and finally refilled with 100 μL of HBSS containing different concentrations of the TCA under study, and pre-incubated for 5 min. Plates were then placed in the cell plate stage of the fluorescent imaging plate reader (Molecular Devices, Sunnyvale, CA, USA). A baseline consisting of 5 measurements of 0.4 s each was recorded. ( ± )-Epibatidine (0.1 μM) was then added from the agonist plate to the cell plate using the 96-tip pipettor simultaneously to fluorescence recordings for a total length of 3 min. The laser excitation and emission wavelengths are 488 and 510 nm, at 1 W, and a CCD camera opening of 0.4 s.

### 2.3. Whole-cell patch-clamp recordings of brain slices

Brain slices were prepared as previously described (Vázquez-Gómez et al., 2014). Whole-cell voltage-clamp recording of interneurons from the *stratum radiatum* hippocampal CA1 area were performed with a PC-ONE Patch/Whole Cell Clamp (Dagan Corporation, MN, USA) using a Digidata 1440 A acquisition system driven with pClamp 10 (Molecular Devices, CA, USA). Patch-clamp electrodes had a resistance of 3–7 MΩ when filled with the solution (in mM): 140 KCl, 10 Hepes, 2 MgCl$_2$, 0.5
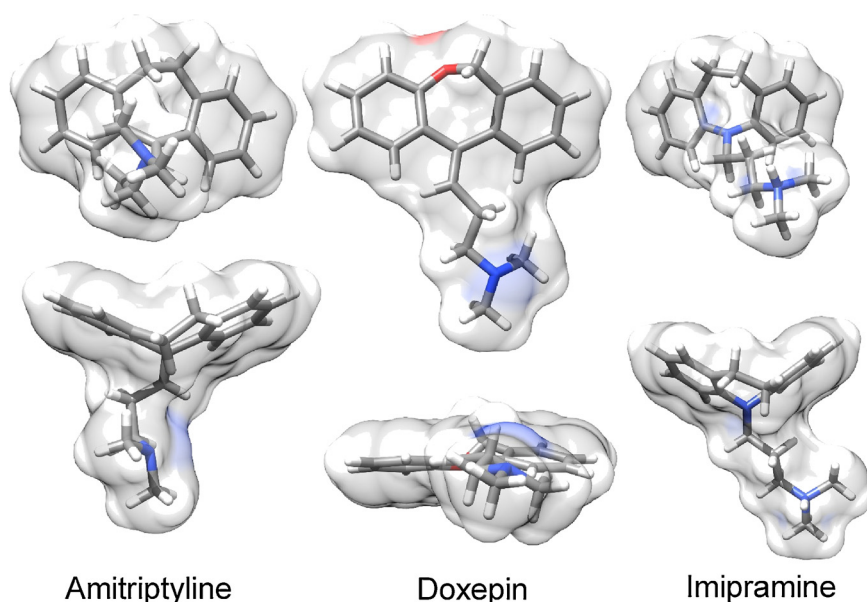


Fig. 1. Molecular structure of TCAs. The upper panel shows amitriptyline, doxepin, and imipramine viewed parallel to their tricyclic moiety, while the lower panel is a 90° rotation view from the former. Color scheme for atoms and surfaces: carbons (gray), nitrogens (blue), oxygens (red), and hydrogen (white) (For interpretation of the references to colour in this figure legend, the reader is referred to the web version of this article).

Amitriptyline          Doxepin          Imipramine

**(A)**



**(B)**



**Fig. 2.** Effect of TCAs on ( ± )-epibatidine-induced $Ca^{2+}$ influx in GH3-h$\alpha$7 cells. (A) The increase in intracellular calcium elicited by 0.1 μM ( ± )-epibatidine (■) was decreased by 10 μM imipramine (▲). (B) Increased concen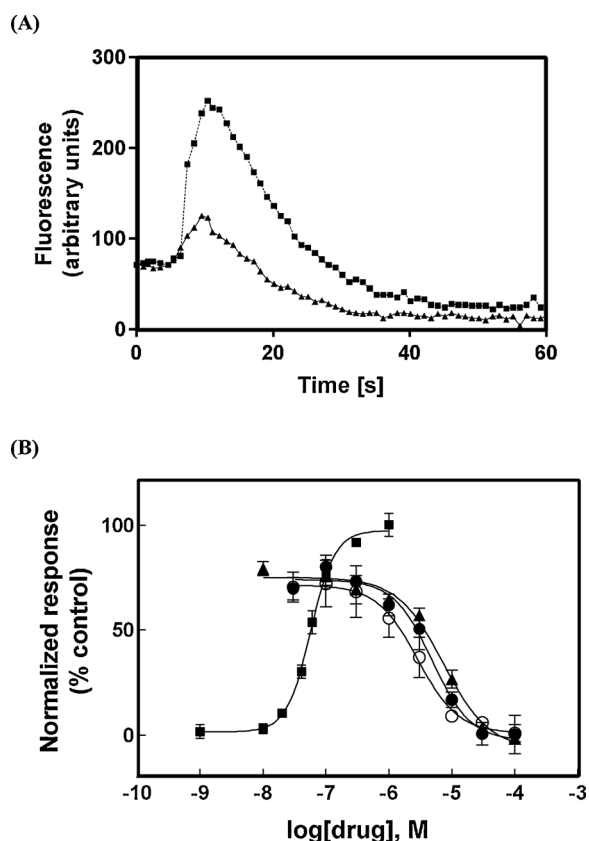trations of ( ± )-epibatidine (■) activate h$\alpha$7 AChRs with potency $EC_{50}$ = 52 ± 4 nM (n = 4). Subsequently, cells were pre-treated with several concentrations of amitriptyline (○), imipramine (▲), and doxepin (●), followed by addition of 0.1 μM ( ± )-epibatidine. Response was normalized to the maximal ( ± )-epibatidine response which was set as 100%. The plots are representative of 4–6 determinations, where the error bars are S.D. The calculated $IC_{50}$ and $n_H$ values were summarized in Table 1.

$CaCl_2$, 10 EGTA, 2 MgATP, pH 7.4. Data were acquired in a PC using a Digidata 1440 A AD converter at a sampling rate of 10 kHz.

To determine the effect of imipramine on hippocampal $\alpha$7* AChRs, 10 mM choline (Ch) puffs (2–5 psi, 500 ms) were applied on interneurons through a fine tip glass micropipette placed ∼10 μm from the recorded cell by using a picopump (PV830, WPI, FL, USA). Ch-puffs were applied every 5 min, before (basal condition), during imipramine was added to the bath solution (∼10 min), and after washing (5 min) (recovery condition). The Ch-induced current amplitude was measured as a function of recording time. The concentration–response relationship was fitted using the Prism software (GraphPad Software, San Diego, CA). The inhibitory potency ($IC_{50}$) for imipramine was obtained by using the Hill equation (Weiss, 1997). To determine whether imipramine-induced inhibition is voltage-dependent or not, the interneurons were maintained at a potential of -70 or −20 mV.

### 2.4. Voltage clamp recordings on oocytes expressing α9α10 AChRs

Rat $\alpha$9 and $\alpha$10 subunits were expressed in *Xenopus* oocytes as previously described (Ballestero et al., 2005). Electrophysiological recordings were performed at −70 mV using two-electrode voltage-clamp (Ballestero et al., 2005; Elgoyhen et al., 2001). Oocytes were pre-incubated for 2 min with imipramine before adding acetylcholine (ACh) and imipramine. The average peak amplitude of three control ACh responses just before the exposure to imipramine was used to normalize

the amplitude of each test response in the presence of the drug. To determine the mechanism of inhibition of imipramine, two approaches were used: (1) current-voltage (I–V) relationships were obtained by applying 2-s voltage ramps from -120 to 50 mV, 10 s after the peak response to 10 μM ACh from a holding potential ($V_{hold}$) of −70 mV. Leakage correction was performed by subtraction of the I–V curve obtained before the application of ACh, and (2) the $EC_{50}$ values for ACh were obtained in the absence and presence of 0.6 μM imipramine.

### 2.5. Radioligand competition binding experiments using hα7 AChRs in different conformational states

To determine the binding affinity of TCAs (Fig. 1) for h$\alpha$7 AChRs in different conformational states, [$^3$H]imipramine competition binding experiments were performed using SHSY5Y-h$\alpha$7 cell membranes prepared as described previously (Arias et al., 2010a). In this regard, h$\alpha$7 AChR-containing membranes (1.5 mg/mL) were incubated (2 h) with 15 nM [$^3$H]imipramine in the presence of 0.1 μM $\alpha$-BTx [receptors are mainly in the resting state (Moore and McCarthy, 1995)] or 1 μM (-)-nicotine (receptors are mainly in the desensitized state). To determine whether imipramine interacts with the agonist sites, additional [$^3$H]MLA competition experiments were performed using 5.2 nM [$^3$H] MLA in the absence of any other ligand by following the same procedure. Nonspecific binding was determined in the presence of 200 μM imipramine and 10 μM MLA, respectively. The radioactivity was determined as previously described (Arias et al., 2010a). The $IC_{50}$ value for imipramine obtained from the [$^3$H]MLA competition experiments was transformed into its inhibition constant ($K_i$) using the Cheng–Prusoff relationship (Cheng and Prusoff, 1973) and $K_d^{MLA}$ = 1.86 nM (Davies et al., 1999).

### 2.6. Molecular docking and molecular dynamics simulations

The $\alpha$7 and $(\alpha9)_2(\alpha10)_3$ AChRs were first built using the X-ray structure (PDB ID: 5KX) of the human $\alpha4\beta2$ AChR at 3.9 Å resolution (Morales-Perez et al., 2016). Imipramine in the protonated state (i.e., protonated at physiological pH) was modeled using VEGA ZZ and subsequently docked at the h$\alpha$7 and h$\alpha$9$\alpha$10 AChRs using AutoDock Vina. Protocols for minimization, partial charge calculations and docking were carried out as previously described (Arias et al., 2016).

To determine the stability of each pose within its predicted docking site, 20-ns molecular dynamics (MD) simulations were performed as previously described (Arias et al., 2016), using NAMD and CHARMM force field, and VEGA ZZ as interface. Poses with variance (VAR) RMSD < 1 during the last third of the MD were used.

### 2.7. Calculation of the theoretical binding energies

Theoretical binding energies (TBE), measured from the individual poses at the end of the MD, were calculated using molecular mechanics (Tirado-Rives and Jorgensen, 2006). The TBE values are estimations used only for comparative purposes among receptors and its respective sites, and do not intend to represent absolute binding energies. More negative TBE values indicate higher theoretical binding affinities (TBA).

## 3. Results

### 3.1. Inhibitory potency of TCAs at hα7 AChRs

Pre-incubation with each TCA subsequently inhibited the observed ( ± )-epibatidine-induced h$\alpha$7 AChR activation with high effectiveness. Fig. 2A shows the fluorescence traces produced by 0.1 μM ( ± )-epibatidine, which were practically 100% inhibited by 10 μM imipramine. The concentration-response curve analyses (Fig. 2B) gave inhibitory potencies ($IC_{50}$ in μM) that follow the rank order: amitriptyline

**Table 1**
Inhibitory potency ($IC_{50}$) of TCAs at α7, α9α10, and hippocampal α7*AChRs.

| AChR subtype | Method | TCA | $IC_{50}$, μM | $n_H$ |
|---|---|---|---|---|
| α7[a] | $Ca^{2+}$ influx on GH3-hα7 cells | Amitriptyline | 2.7 ± 0.3 | 2.00 ± 0.69 |
| | | Doxepin | 5.9 ± 1.1 | 2.28 ± 0.52 |
| | | Imipramine | 6.6 ± 1.0 | 2.01 ± 0.44 |
| Hippocampal α7* AChRs[b] | Voltage-clamp on hippocampal CA1 interneurons | Imipramine | 42.2 ± 8.5 | 1.20 ± 0.27 |
| α9α10[c] | Voltage-clamp on oocytes expressing α9 and α10 subunits | Imipramine | 0.54 ± 0.05 | 0.70 ± 0.05 |

$n_H$, Hill coefficient.

  [a] Values were obtained from Figures 2B[a], 3B[b], and 4B[c], respectively.

  [b] Values were obtained from Figures 2B[a], 3B[b], and 4B[c], respectively.

  [c] Values were obtained from Figures 2B[a], 3B[b], and 4B[c], respectively.

(2.7 ± 0.3) > doxepin (5.9 ± 1.1) ~ imipramine (6.6 ± 1.0) (Table 1). The result showing that the $n_H$ values are higher than unity (Table 1) indicated that the inhibitory process is mediated by a co-operative mechanism.

### 3.2. Imipramine inhibits rat hippocampal α7*AChRs in a voltage-dependent manner

The electrical activity of native α7* AChRs was first recorded by applying local puffs of 10 mM Ch, a selective α7-agonist (Liu et al., 2012), at 5-min intervals, onto interneurons from the rat *stratum radiatum* hippocampal CA1 area (Fig. 3A). The activity of imipramine was determined on Ch-induced current amplitudes as a function of recording time before and during imipramine application (10 min) and after washing (5 min) (i.e., recovery) (Fig. 3A). The concentration-response curve (Fig. 3B) gave the following values: $IC_{50}$ = 42.2 ± 8.5 μM and $n_H$ near unity (Table 1), where the latter value indicates a non-cooperative mechanism of inhibition.

The membrane potential dependence was determined on hippocampal α7* AChRs, by comparing the inhibition elicited by 50 μM imipramine on Ch-induced currents between −70 and −20 mV (Fig. 3C). At −70 mV, the $I_{Ch+Imi}/I_{Ch}$ ratio was 0.46 ± 0.03, whereas at −20 mV, this ratio was 0.84 ± 0.12. These inhibitory values were statistically different, being stronger at -70 than at −20 mV (Student's t-test, p < 0.05), indicating that the imipramine-induced inhibition depends on the membrane potential.

### 3.3. Imipramine inhibits rα9α10 AChRs in a voltage-independent and competitive manner

Imipramine inhibited ACh (10 μM)-evoked rα9α10 AChR activity in a concentration-dependent manner (Figs. 4A,B), giving an $IC_{50}$ value of 0.54 ± 0.05 μM (Table 1). The observed $n_H$ value close to unity (Table 1) indicated that the inhibitory process is mediated by a non-cooperative mechanism.

To study further the inhibitory mechanism of imipramine, two approaches were used. First, the inhibitory activity of 1 μM imipramine was determined at different membrane potentials, as shown in the representative I/V curves (Fig. 4C). The responses were equally inhibited (p = 0.1) at both negative (−90 mV) ($I/I_{max}$: 50 ± 4.1%) and positive (+40 mV) potentials (60 ± 3.5%), indicating that the imipramine-induced inhibition was voltage-independent. Secondly, the activity of increasing concentrations of ACh was determined in the absence and presence of 0.6 μM imipramine, corresponding to its $IC_{50}$ value (Fig. 4D). The competition curves showed that imipramine produced a parallel rightward shift of ACh-evoked responses. A significant increase of the ACh $EC_{50}$ value (17.6 ± 1.5 μM) was observed in the presence of
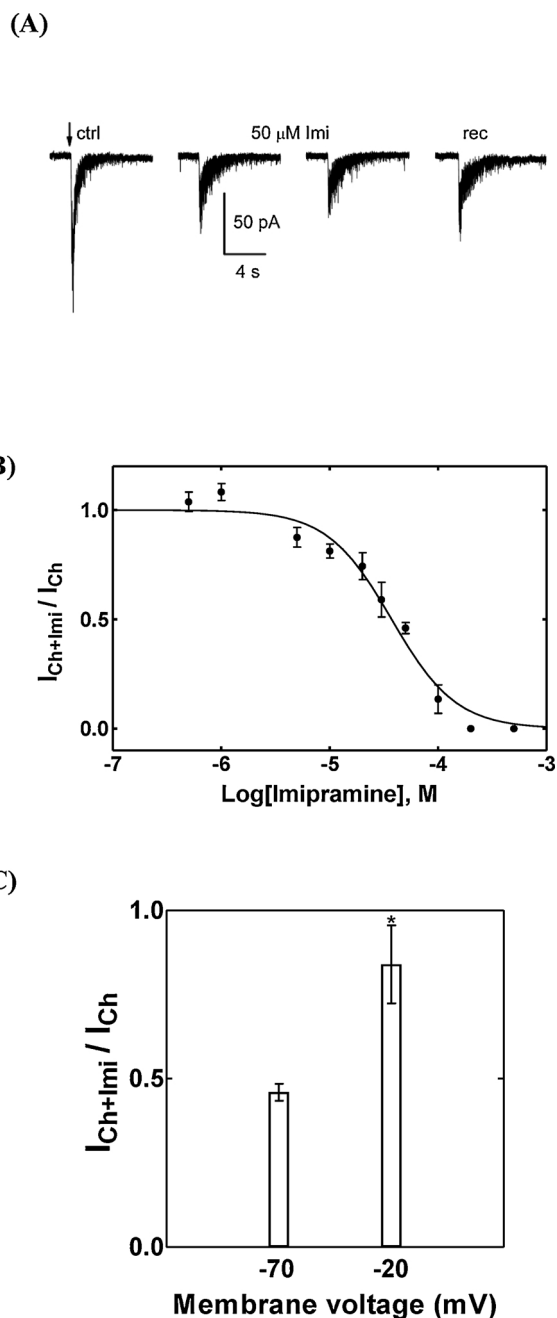
**(A)**



**(B)**



**(C)**



**Fig. 3.** Inhibitory effect of imipramine on choline (Ch)-induced currents at hippocampal CA1 interneurons. (A) Representative Ch-induced currents inhibited by imipramine. Choline puffs (2–5 psi, 500 ms) were applied at 5-min intervals before (Ctr) and during the application of 50 μM imipramine (Imi) (10 min), and after washing (5 min) [i.e., recovery (rec)]. The holding potential of the interneurons was −70 mV. (B) Concentration-response curve (mean ± SD) for the inhibitory activity of imipramine on hippocampal interneurons (n = 4–5). The calculated $IC_{50}$ and $n_H$ values were summarized in Table 1. (C) Voltage dependence of imipramine inhibitory effects at hippocampal interneurons (n = 4). The columns (mean ± SD) represent the ratio $I_{Ch+Imi}$ / $I_{Ch}$ at the holding potential of -20 and −70 mV, respectively. The asterisk indicates significant statistical difference (Student's t-test; p < 0.05).

imipramine (36.1 ± 2.7 μM) (p = 0.0001), with no changes in agonist maximal responses and $n_H$ values (Table 2), supporting a competitive mechanism of inhibition.
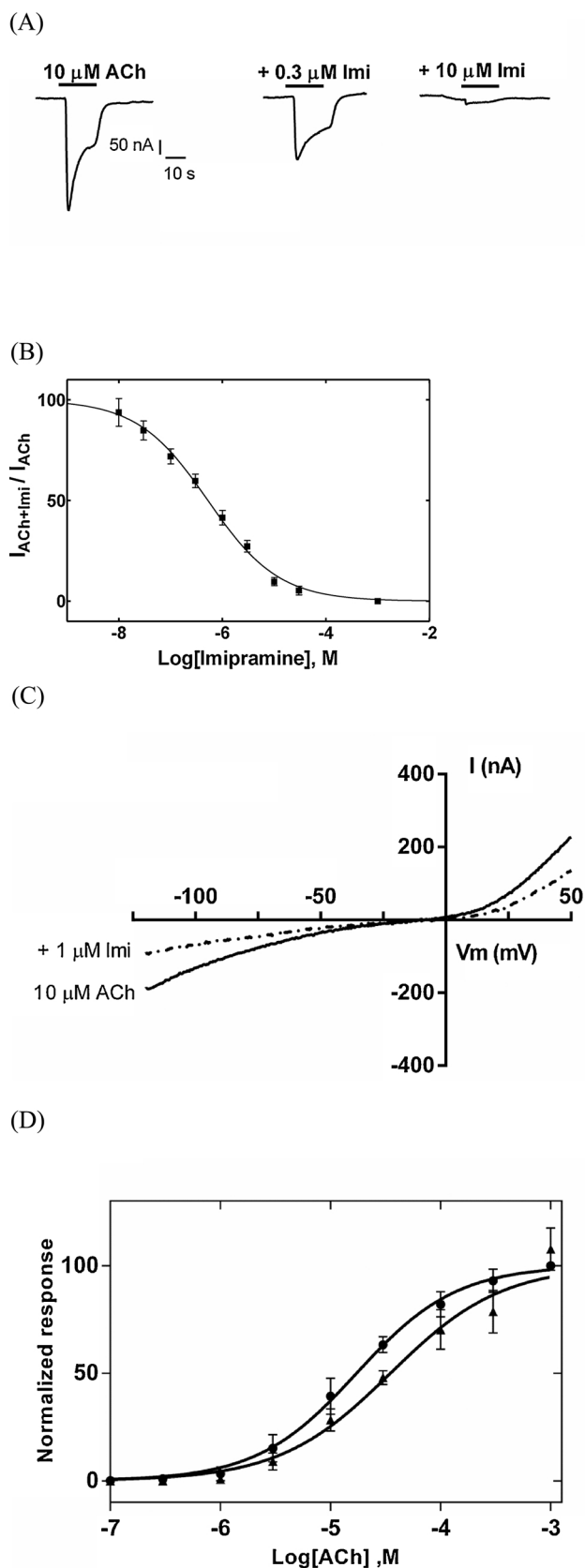
(A)



(B)



(C)



(D)



**Fig. 4.** Effect of imipramine on acetylcholine (ACh)-evoked activity at rα9α10 AChRs expressed in *X. oocytes*. (A) Responses of rα9α10 AChRs elicited by 10 μM AChare diminished by increasing concentrations of imipramine. (B). Inhibition curve performed by the co-application of 10 μM ACh and increasing concentrations of imipramine (n = 7). Responses (mean ± SEM) were normalized to that elicited by 10 μM ACh (its $EC_{50}$ value) which was set as 100%. The calculated $IC_{50}$ and $n_H$ values were summarized in Table 1. (C) Current-voltage relationships (n = 4) were obtained by applying 2-s voltage ramps from -120 to + 50 mV, 10 s after the peak response to 10 μM ACh from a holding potential ($V_{hold}$) of −70 mV, in the presence and absence of 1 μM imipramine. No statistical difference was obtained (Student's t-test; p = 0.1). (D) Concentration-response curves for ACh in the absence (●) and presence (▲) of 0.6 μM imipramine (n = 6). Responses (mean ± SEM) were normalized to that elicited by 10 μM ACh which was set as 100%. The $EC_{50}$ values for ACh in the absence and presence of imipramine were summarized in Table 2. A statistical difference was obtained (p = 0.0022).

**Table 2**
Potency of ACh ($EC_{50}$) in the absence and presence of imipramine at the α9α10AChR.

| ACh | $EC_{50}$ (μM) | $n_H$ |
|---|---|---|
| No imipramine | 17.6 ± 1.5 | 0.96 ± 0.04 |
| 0.6 μM imipramine | 36.1 ± 2.7 | 0.86 ± 0.06 |

Values obtained from Fig. 4D.

### 3.4. Interaction of TCAs with the imipramine and agonist binding sites at the hα7 AChR

To compare the binding affinity of TCAs for hα7 AChRs in different conformational states, the activity of imipramine on [³H]imipramine binding to hα7 AChRs was determined in the resting and desensitized states (Fig. 5A). TCAs inhibited 100% [³H]imipramine binding to hα7 AChRs in different conformational states (Figs. 5A,B). The $IC_{50}$ value (in μM) for imipramine at resting α7 AChRs (1.6 ± 0.2) is not statistically different from that obtained in the desensitized state (1.9 ± 0.3) (p > 0.05) (Table 3). Thus, the $IC_{50}$ values for amitriptyline and doxepin were determined using hα7 AChRs in the resting state. Comparing the $IC_{50}$ values in the resting state (Table 3), the following rank sequence was obtained: imipramine (1.6 ± 0.2) > amitriptyline (2.4 ± 0.3) > doxepin (4.9 ± 0.6). The $n_H$ values are lower than unity, but higher than 0.5 (Table 3), supporting a non-cooperative mechanism of inhibition.

The [³H]MLA competition binding experiments indicated that although imipramine binds to the agonist sites, its affinity is 44-fold lower than that for the [³H]imipramine sites (Fig. 5C; Table 3). The calculated $n_H$ value is close to unity (Table 3), indicating that the TCAs inhibit [³H]MLA binding in a non-cooperative manner.

### 3.5. Molecular docking of imipramine to the hα7 and hα9α10 AChRs

In the hα7 model, three stable poses for imipramine were found by molecular docking, located at two partially overlapping luminal sites and one extracellular-transmembrane (ECD-TMD) junctional site (Fig. 6A). In the h(α9)$_2$(A10)$_3$ model, imipramine interacted with the orthosteric and luminal sites (Fig. 7). The residues interacting with imipramine at each docking site, as well as the average RMSD (i.e., measures the deviation of the pose from the original docking position) and variance (VAR) (i.e., indicates the stability of the pose within its final location) values (Fig. S1A; Supplementary Material), and the TBE estimations, are summarized in Tables 4(for α7) and 5 (for α9α10), respectively.

In the hα7 model, the orientation 1 is close to the cytoplasmic side of the ion channel, located between the serine (2′) and leucine (9′) rings (Fig. 6B). Imipramine made contacts with M2 residues, including S241 (2′), I244 (5′), T245 (6′; threonine ring), and L248 (9′) and forms two
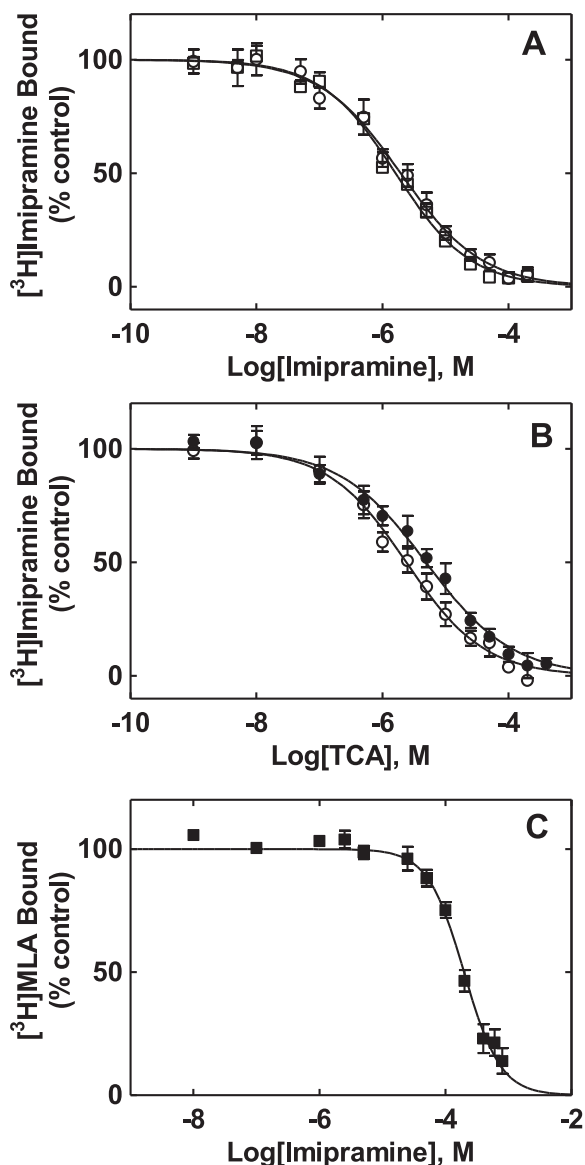
**Fig. 5.** Interaction of TCAs to the agonist and noncompetitive binding sites at the hα7 AChR. (A) The interaction of TCAs with the noncompetitive sites was determined by [$^3$H]imipramine competition binding assays using hα7 AChRs in different conformational states. hα7 AChR-containing SH-SY5Y membranes (1.5 mg/mL) were equilibrated (2 h) with 15 nM [$^3$H]imipramine in the presence of 0.1 μM α-BTx [α-BTx-bound/resting state (□)] or 1.0 μM (-)-nicotine [nicotine-bound/desensitized state (○)], and increasing concentrations of imipramine. (B) [$^3$H]Imipramine competition binding experiments for amitriptyline (○) and doxepin (●) in the absence of any ligand (receptors are mainly in the resting state). Nonspecific binding was determined at 200 μM imipramine. (C) The interaction of imipramine with the agonist binding sites was determined by [$^3$H]MLA competition binding assays. Nonspecific binding was determined at 10 μM MLA. (A–C) Each plot is the combination of 2–3 separated experiments each one performed in triplicate. The IC$_{50}$ and n$_H$ values were obtained by nonlinear least-squares fit. The imipramine IC$_{50}$ value for the [$^3$H] MLA sites was transformed to its K$_i$ value. The IC$_{50}$, K$_i$, and n$_H$ values were summarized in Table 3.

H-bonds with the side and main chains O of one of the T245 residues. In orientation 2, imipramine interacted with M2 residues between the leucine and valine (13′) rings, including L248 (9′), S249 (10′), T251 (12′), V252 (13′), and F252 (14′) (Fig. 6C). In the ECD-TMD junction site, imipramine interacted with ECD residues belonging to the β6-β7 loop (i.e., F135, P136 and F137), as well as with residues from the M1 (i.e., L216, C219, and V220), M3 (i.e., L270, I271 and Y274), and M4

(i.e., T461, I464, and L465) segments (Fig. 6D). Imipramine is stabilized by intra- and inter-molecular cation-π interactions between the charged amino nitrogen of the ligand side chain, and one of the aromatic rings of its tricycle moiety, and with the Y274 aromatic side chain, respectively.

In the orthosteric site from the hα9α10 model, imipramine is located at the interface between the α10(+) or principal component and α9(-) or complementary component, as in the case of agonists and competitive antagonists (Arias, 2012). This interaction involved several α10 residues, including Y95 (β4-β5 loop), W151 (β7-β8 loop), Y192 and G193 (H-bonds), C195 (β9-β10 loop), and Y199 (β10 sheet; π-π interactions), as well as α9 residues, comprising R59 (H-bond) and W57 (cation-π and H-bond interactions) (β2 sheet), R81 (β3 sheet; H-bond), V111 (β5 sheet), D121 (H-bond) and T119 (β6 sheet), and S170 and D171 (β8-β9 loop; both form H-bonds) (Fig. 7B,C; Table 5). The luminal site for imipramine, located between positions 5′ and 13′ (Fig. 7 A), is formed by M2 residues from both α9 and α10 subunits, including V248 (5′), T249 (6′), L252 (9′), A253 (10′), and V256 (13′), as well as with α9-T255 (12′) (Table 5).

## 4. Discussion

In this study, the inhibitory activity of TCAs was compared between hα7, rα9α10, and hippocampal α7* AChRs by using a combination of Ca$^{2+}$ influx and voltage clamp recordings. To determine the mechanism (s) of inhibition of imipramine at these AChRs, additional functional and structural studies were performed.

The Ca$^{2+}$ influx results indicated that TCAs inhibit (±)-epibatidine-activated hα7 AChRs with potencies (IC$_{50}$s in μM) that follow the rank order: amitriptyline (2.7 ± 0.3) > doxepin (5.9 ± 1.1) ~ imipramine (6.6 ± 1.0). The activity for imipramine as well as the observed sequence is practically the same as that obtained for other AChR subtypes (Arias et al., 2010b, 2010c; Feuerbach et al., 2005; Gumilar et al., 2003; López-Valdés et al., 2002; López-Valdés and García-Colunga, 2001). This suggests that the inhibitory potency of each TCA depends mainly on its molecular structure and less on the physico-chemical properties of the binding sites at each nAChR subtype.

Interestingly, the voltage-clamp results showed that imipramine inhibits Ch-evoked currents from hippocampal interneurons in a voltage-dependent manner. Since Ch is a selective α7-agonist (Liu et al., 2012), the observed inhibitory activity of imipramine is ascribed to hippocampal α7* AChRs. These results are in agreement with previous works showing that the imipramine- and clomipramine-induced inhibition of α2β4 and muscle-type AChRs is voltage-dependent (López-Valdés et al., 2002; López-Valdés and García-Colunga, 2001).

The results on rat hippocampal α7* nAChRs showed that imipramine inhibits endogenous receptors with relatively low potency (42.2 ± 8.5 μM), and by a non-cooperative mechanism (n$_H$ = 1.20 ± 0.27). Based on intrinsic differences in the used methods {drug potency is usually decreased in a tissue slice [e.g., see (Arias et al., 2017)] compared to Ca$^{2+}$ influx assays using GH3-hα7 cells} and receptor species (rat *vs* human α7 AChRs), a direct comparison between the calculated potencies cannot be done. Nevertheless, the cooperative interaction of imipramine at hα7 nAChRs (n$_H$ = 2.01 ± 0.44) might suggest several binding sites, as observed in our docking results (see below), whereas the interaction to endogenous rat α7* nAChRs (including α7β2 nAChRs) could be mediated by a single site.

The rat brain concentration of imipramine after chronic treatment (i.e., daily i.p. injection of 10 mg/kg imipramine for 14 days) reaches values as high as ~25 μM (Daniel et al., 1981). Considering that the tissue distribution and pharmacokinetics properties of imipramine in rodents are very similar to that in humans, the determined brain concentration of this antidepressant will be enough to decrease, at least partially, the activity of hippocampal α7* AChRs. A possible implication of imipramine-induced inhibition of α7* AChRs in *stratum radiatum* interneurons is a decrease of GABA release and consequently a

**Table 3**

Binding affinity of TCAs for the agonist and noncompetitive antagonist binding sites at the hα7 AChR.

| TCA | [³H]Imipramine[a] | | | | [³H]MLA | |
|---|---|---|---|---|---|---|
| | Resting state (α-BTx-bound state) | | Desensitized state(Nicotine-bound state) | | No ligand | |
| | IC$_{50}$, μM | n$_H$ | IC$_{50}$, μM | n$_H$ | K$_i$, μM | n$_H$ |
| Imipramine | 1.6 ± 0.2 | 0.73 ± 0.05 | 1.9 ± 0.3 | 0.68 ± 0.06 | 70 ± 4[b] | 1.20 ± 0.08 |
| Amitriptyline | 2.4 ± 0.3 | 0.70 ± 0.06 | – | – | – | – |
| Doxepin | 4.9 ± 0.6 | 0.64 ± 0.05 | – | – | – | – |

n$_H$, Hill coefficient.

[a] The IC$_{50}$ values were obtained from Fig. 5A (imipramine) and Fig. 5B (amitriptyline and doxepin), respectively.

[b] The K$_i$ value for imipramine was obtained from Fig. 5C.

disinhibition of CA1 pyramidal neurons. Accordingly, imipramine may alter the inhibitory mechanisms that control the activity of these interneurons, considered fundamental in maintaining neuronal circuit oscillations, which seem to be disrupted during depression (Chamberland and Topolnik, 2012). Nevertheless, based on results showing that agonist-induced α7 AChR activation, but not inhibition, decreases inflammation, an alternative hypothesis has been developed where α7 agonist-decreased inflammation might alleviate psychiatric disorders such as depression (Kalkman and Feuerbach, 2016). This concept is reinforced by additional studies indicating that positive allosteric modulators that potentiate, but not desensitize, α7 AChR

function have both anti-inflammatory (Bagdas et al., 2015) and anti-depressant-like (Arias et al., 2015) activity.

The results from the [³H]imipramine competition binding experiments indicated that TCAs do not discriminate between the desensitized and resting hα7 AChRs. These studies also showed that their affinities for the resting hα7 AChR follow the rank order: imipramine > amitriptyline > doxepin. The same trend was observed for the *Torpedo* (Gumilar et al., 2003), hα4β2 (Arias et al., 2010b), and hα3β4 (Arias et al., 2010c) AChRs. The different rank order between binding affinities and inhibitory potencies could be explained considering that although imipramine binds with relatively higher affinity to its site(s) at
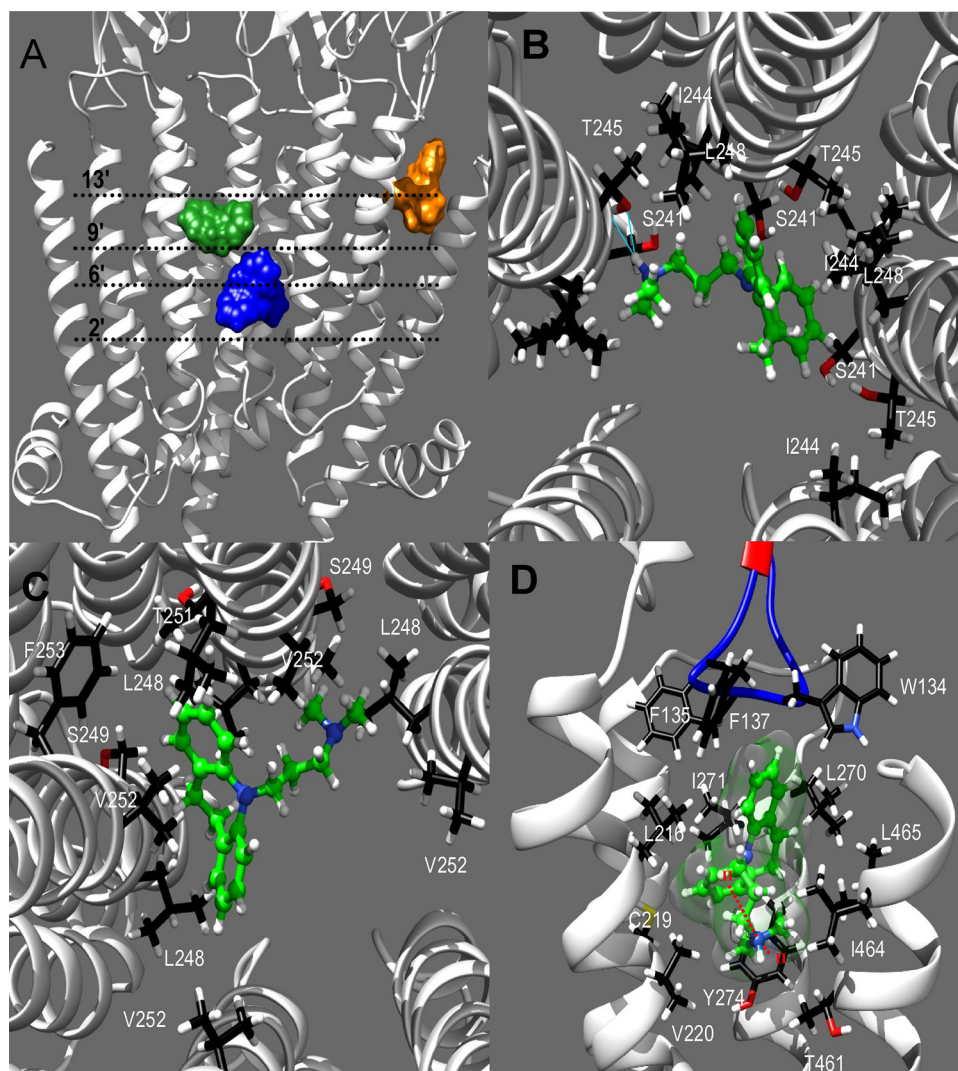


**Fig. 6.** Docking sites for protonated imipramine at the α7 AChR model. (A) Imipramine (as molecular surface) interacted with two partially overlapping luminal sites, one located between the serine (2′) and leucine (9′) rings [orientation 1 (blue)], and another located between the leucine and valine (13′) rings [orientation 2 (green)]. Imipramine also interacted with a non-luminal site located within the ECD-TMD junction [ECD-TMD site (orange)]. (B) In orientation 1, imipramine (as ball and sticks) interacted with S241 (2′), T245 (6′; threonine ring) with which establishes two H-bonds, I244 (5′), and L248 (9′). Light blue lines represent H-bonds. (C) In orientation 2, imipramine interacted with L248 (9′), S249 (10′), T251 (12′), V252 (13′), and F252 (14′). (D) In this ECD-TMD site, imipramine (as ball and sticks surrounded by its molecular surface) interacted with residues belonging to the β6-β7 loop (in blue; i.e., F135, P136 and F137), M1 (i.e., L216, C219, and V220), M3 (i.e., L270, I271 and Y274), and M4 (i.e., T461, I464, and L465). The red dotted lines indicate a cation-π interaction between the side chain of the charged amino nitrogen of imipramine and the Y274 aromatic side chain, and also with one of the aromatic rings of imipramine itself. The residues involved in the binding (as sticks) (listed in Table 4) are labeled by using the one letter code and amino acid sequence number. Color scheme for atoms: carbons (green for imipramine, black for receptor residues), nitrogens (blue), oxygens (red), sulphur (yellow), and hydrogen (white). (For interpretation of the references to colour in this figure legend, the reader is referred to the web version of this article).
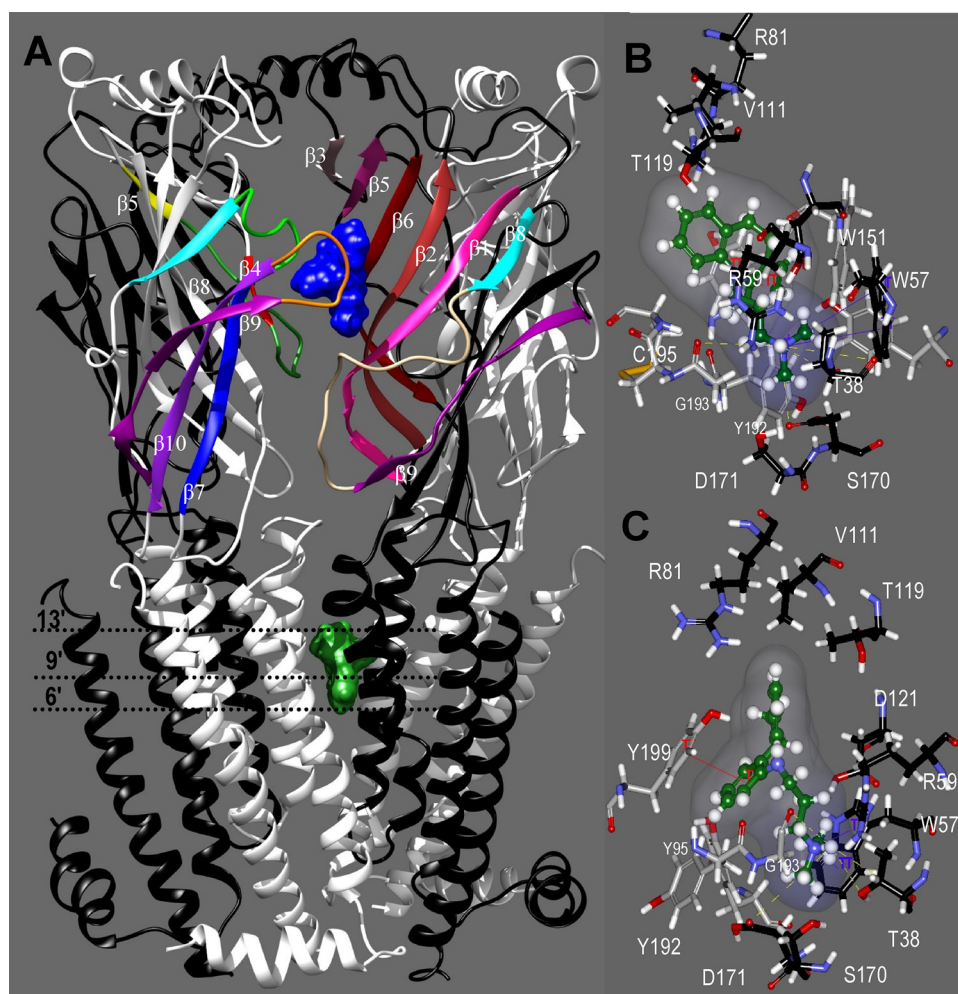
**Fig. 7.** Docking sites for protonated imipramine at the h(α9)₂(α10)₃ AChR model. (A) Imipramine (as molecular surface) interacted with the orthosteric sites (blue) and a luminal site (green). One α10 subunit was omitted for clarity. The orthosteric site (blue) comprises the principal component (+), formed by α10 residues (white), and the complementary component (-) formed by α9 residues (black). Characteristic secondary structures are differentially colored for identification: α10: β4 sheet (red), β4-β5 loop (dark green), β5 sheet (yellow), β7 sheet (blue), β7-β8 loop (light green), β8 sheet (cyan), β9 sheet (dark magenta), β9-β10 loop (orange), β10 sheet (purple); α9: β1 sheet (pink), β2 sheet (brown), β3 sheet (light pink), β5 sheet (yellow), β6 sheet (dark red), β8 sheet (cyan), β8-β9 loop (light brown), β9 sheet (dark magenta). The luminal site (green) is located between the threonine (6′) and valine (13′) rings. The involved residues are listed in Table 5. (B) Detailed view of protonated imipramine (as ball and sticks and carbons in green) interacting with the orthosteric site. The network of H-bonds between the protonated N of imipramine and Y192, G193, R59, W57; S170 and D171, is shown as yellow lines. The purple lines indicate cation-π interactions between both rings of W57 and the protonated N of imipramine. (C) A different view of the orthosteric site allows us to see the π-π interaction (red line) between Y199 and one of the aromatic rings of imipramine. (For interpretation of the references to colour in this figure legend, the reader is referred to the web version of this article).

**Table 4**
Docking parameters for imipramine interacting with the hα7 model.

| Site | TBE[a] (kcal/mol) | RMSD[b] (VAR) | Domain | Subdomain | Residue (type of interaction) | M2 position (ring) |
|---|---|---|---|---|---|---|
| ECD-TMD | −47 | 0.708 (0.006) | ECD | β6-β7 loop | W134 | |
| | | | | | F135 | |
| | | | | | F137 | |
| | | | TMD | M1 | L216 | |
| | | | | | C219 | |
| | | | | | V220 | |
| | | | | M3 | L270 | |
| | | | | | I271 | |
| | | | | | Y274 (cation-π) | |
| | | | | M4 | T461 | |
| | | | | | I464 | |
| | | | | | L465 | |
| Luminal orientation 1 | −40 | 0.557 (0.010) | Ion channel | M2 | S241 | 2′ (serine) |
| | | | | | I244 | 5′ |
| | | | | | T245 (H-bond) | 6′ (threonine) |
| | | | | | L248 | 9′ (leucine) |
| Luminal orientation 2 | −40 | 1.872 (0.003) | Ion channel | M2 | L248 | 9′ (leucine) |
| | | | | | S249 | 10′ |
| | | | | | T251 | 12′ |
| | | | | | V252 | 13′ (valine) |
| | | | | | F253 | 14′ |

[a] The more negative the TBE (theoretical binding energy) values, the higher the theoretical binding affinities (TBA).

[b] RMSD values and their variance (VAR) were calculated during the last third of the MD simulations (see Supplementary Material).

**Table 5**
Docking parameters for imipramine interacting with the hα9α10 model.

| Site | TBE[a](kcal/mol) | RMSD[b] (VAR) | Domain | Subdomain | Subunit | Residue (type of interaction)[c] | Position[d](ring) |
|------|------------------|---------------|--------|-----------|---------|----------------------------------|-------------------|
| Orthosteric | −73 | 0.63 (0.001) | ECD | β4-β5 loop | α10 | Y95 | + |
| | | | | β7-β8 loop | | W151 | + |
| | | | | β9-β10 loop | | Y192 (HB)(H−bond) | |
| | | | | | | G193 (HB) (H−bond) | |
| | | | | | | C195 | + |
| | | | | β10 Sheet | | Y199 (π-π) | + |
| | | | | β1 Sheet | α9 | T38 (H−bond) | |
| | | | | β2 Sheet | | R59 (HB) (H-bond) | − |
| | | | | | | W57(HB;C-π)(cation-π) | − |
| | | | | β3 Sheet | | R81(HB) | |
| | | | | β5 Sheet | | V111 | − |
| | | | | β6 Sheet | | D121 (HB) (H−bond) | − |
| | | | | | | T119 | − |
| | | | | β8-β9 loop | | S170 (HB) (H−bond) | |
| | | | | | | D171 (HB) (H−bond) | |
| Luminal | −44 | 0.43 (0.049) | Ion channel | M2 | α10 | V248 | 5′ |
| | | | | | | T249 | 6′ (threonine) |
| | | | | | | L252 | 9′ (leucine) |
| | | | | | | A253 | 10′ |
| | | | | | | V256 | 13′ (valine) |
| | | | | | α9 | V248 | 5′ |
| | | | | | | T249 | 6′ (threonine) |
| | | | | | | L252 | 9′(leucine) |
| | | | | | | A253 | 10′ |
| | | | | | | T255 | 12′ |
| | | | | | | V256 | 13′(valine) |

[a] The more negative the TBE (theoretical binding energy) values, the higher the theoretical binding affinities (TBA).

[b] RMSD values and their variance (VAR) were calculated during the last third of the MD simulations (see Supplementary Material).

[c] The specific residue-ligand interactions are indicated. HB: H−bond; C-π: cation-pi; π-π: pi-pi.

[d] The relative M2 position (ring) is indicated for the luminal site, whereas the residue location at the (+) or (−) side of the orthosteric site interface is included.

the hα7 AChR, its cellular response is less efficient compared to that for the other used TCAs. On the other hand, when the affinity results are compared to that obtained from structurally and functionally different antidepressants, interesting conclusions can be obtained. For example, serotonin selective transporter inhibitors showed none or minimal preference for any α7 AChR conformational state (Arias et al., 2010a), suggesting that structurally-different antidepressants are less susceptible to discriminate between the resting and desensitized states from the α7 AChR compared to other AChR subtypes (Arias et al., 2010a, 2010b, 2010c; Gumilar et al., 2003).

The observed voltage-dependence of the imipramine-induced inhibition of hippocampal α7* AChRs in addition to the [³H]imipramine competition studies described above, support the molecular docking results indicating that imipramine interacts with luminal sites at the hα7 AChR. More specifically, imipramine docked to two overlapping luminal sites, one located between the serine and leucine rings, and another between the leucine and valine rings. This is in agreement with the calculated electric distance (~0.10) for imipramine and clomipramine at the α2β4 and muscle AChRs, consistent with a luminal location for both TCAs (López-Valdés et al., 2002; López-Valdés and García-Colunga, 2001). Similarly, other structurally-different antidepressants overlap the observed imipramine sites at the hα7 AChR, including bupropion [i.e., a site located between the valine and outer (position 20′) rings, and another site between the leucine ring and position 10′ (Vázquez-Gómez et al., 2014)], and fluoxetine [i.e., a site located between the threonine and valine rings (Arias et al., 2010a)]. Moreover, a non-luminal site for imipramine was found at the ECD-TMD junction of the hα7 AChR, supporting the possibility of other allosteric modes of inhibition. In fact, previous results indicated that TCAs can inhibit AChRs by mechanisms involving both open and resting (closed) channels inhibition, slow open channel blockade, and enhancement of receptor desensitization (Gumilar et al., 2003; López-Valdés and García-Colunga, 2001).

The voltage-clamp results indicated that imipramine inhibits rα9α10 nAChRs with relatively high potency (IC$_{50}$ = 0.54 ± 0.05 μM),

and with different mechanism of action compared to that elicited at α7 AChRs. In contrast with the non-competitive and voltage-dependent inhibition of α7 AChRs, the inhibition of α9α10 AChRs is competitive and voltage-independent. This is in agreement with the molecular docking results, showing that imipramine interacted, with high theoretical affinity, with all residues experimentally considered as important for agonist binding, indicating that TCAs preferably interact with the α9α10 AChR orthosteric sites. In other words, the molecular docking data support the experimental results indicating that imipramine inhibits α9α10 and α7 nAChRs by competitive and non-competitive mechanisms, respectively, that imipramine interacts with luminal and non-luminal sites at the α7 nAChR, supporting both blocking and allosteric mechanisms of inhibition, respectively. The described molecular interactions at these two receptor subtypes, including details of the most important ligand moieties, might be utilized to design novel selective antagonists.

Previous works have reported that several antagonists of α9* AChRs produce analgesic and anti-inflammatory activity in animal models, most likely through a peripheral mechanism of action (McIntosh et al., 2009; Romero et al., 2017). The relatively high inhibitory potency of imipramine for α9α10 AChRs might be used to determine the role of α9* AChRs in pain neurotransmission. The administration of a TCA such as imipramine that inhibits α9α10 AChRs with relatively high selectivity could be a valid strategy for the treatment of chronic pain associated with depression symptoms (Sansone and Sansone, 2008). Considering that there is a direct correlation between depression and inflammation (Christmas et al., 2011), it is possible to suggest that the anti-inflammatory activity elicited by α9* nAChR antagonists, including TCAs, might alleviate depressive states. Interestingly, experimental studies have showed a direct connection between the anti-depressant and anti-inflammatory activity of imipramine in the peripheral and central nervous system (Ramirez and Sheridan, 2016).

In conclusion, TCAs inhibit α7, α9α10, and hippocampal α7*AChRs at clinically relevant concentrations and by different mechanisms. The α7 AChR results support a non-competitive mode of inhibition for TCAs

as previously showed for different AChR subtypes, whereas the competitive inhibition observed at α9α10 AChRs suggest subtle differences for this receptor subtype. These results open the door for further studies to determine the clinical impact of each AChR subtype and its respective inhibitory mechanism on the efficacy of TCAs in depression and pain-related diseases.

## Acknowledgement

## Appendix A. Supplementary data

Supplementary material related to this article can be found, in the online version, at doi:https://doi.org/10.1016/j.biocel.2018.04.017.

## References

Arias, H.R., 2012. Molecular interactions between ligands and nicotinic acetylcholine receptors revealed by studies with acetylcholine binding proteins. J. Thermodyn. Catal. 3. http://dx.doi.org/10.4172/2157-7544.1000116.

Arias, H.R., Biała, G., Słomka, M.K., Targowska-Duda, K.M., Biala, G., Kruk-Slomka, M., 2014. Interaction of nicotinic receptors with bupropion: structural, functional, and pre-clinical perspectives. Recept. Clin. Investig. 1, e65. http://dx.doi.org/10.14800/rci.65.

Arias, H.R., Feuerbach, D., Ortells, M.O., 2016. Bupropion and its photoreactive analog (±)-SADU-3-72 interact with luminal and non-luminal sites at human α4β2 nicotinic acetylcholine receptors. Neurochem. Int. 100, 67–77. http://dx.doi.org/10.1016/j.neuint.2016.08.013.

Arias, H.R., Feuerbach, D., Targowska-Duda, K.M., Russell, M., Jozwiak, K., 2010a. Interaction of selective serotonin reuptake inhibitors with neuronal nicotinic acetylcholine receptors. Biochemistry 49, 5734–5742. http://dx.doi.org/10.1021/bi100536t.

Arias, H.R., Jin, X., Feuerbach, D., Drenan, R.M., 2017. Selectivity of coronaridine congeners at nicotinic acetylcholine receptors and inhibitory activity on mouse medial habenula. Int. J. Biochem. Cell. Biol. 92, 202–209. http://dx.doi.org/10.1016/j.biocel.2017.10.006.

Arias, H.R., Rosenberg, A., Targowska-Duda, K.M., Feuerbach, D., Jozwiak, K., Moaddel, R., Wainer, I.W., 2010b. Tricyclic antidepressants and mecamylamine bind to different sites in the human α4β2 nicotinic receptor ion channel. Int. J. Biochem. Cell. Biol. 42, 1007–1018. http://dx.doi.org/10.1016/j.biocel.2010.03.002.

Arias, H.R., Targowska-Duda, K.M., Feuerbach, D., Sullivan, C.J., Maciejewski, R., Jozwiak, K., 2010c. Different interaction between tricyclic antidepressants and mecamylamine with the human α3β4 nicotinic acetylcholine receptor ion channel. Neurochem. Int. 56, 642–649. http://dx.doi.org/10.1016/j.neuint.2010.01.011.

Arias, H.R., Targowska-Duda, K.M., Feuerbach, D., Jozwiak, K., 2015. The antidepressant-like activity of nicotine, but not of 3-furan-2-yl-N-p-tolyl-acrylamide, is regulated by the nicotinic receptor β4 subunit. Neurochem. Int. 87, 110–116.

Bagdas, D., Targowska-Duda, K.M., López, J.J., Pérez, E.G., Arias, H.R., Damaj, M.I., 2015. Antinociceptive and anti-inflammatory properties of 3-furan-2-yl-N-p-tolyl-acrylamide (PAM-2), a positive allosteric modulator of α7 nicotinic acetylcholine receptors, in mice. Anesth. Analg. 121, 1369–1377.

Ballestero, J.A., Plazas, P.V., Kracun, S., Gomez-Casati, M.E., Taranda, J., Rothlin, C.V., Katz, E., Millar, N.S., Elgoyhen, A.B., 2005. Effects of quinine, quinidine, and chloroquine on α9α10 nicotinic cholinergic receptors. Mol. Pharmacol. 68, 822–829. http://dx.doi.org/10.1124/mol.105.014431.

Chamberland, S., Topolnik, L., 2012. Inhibitory control of hippocampal inhibitory neurons. Front. Neurosci. 6, 165. http://dx.doi.org/10.3389/fnins.2012.00165.

Cheng, Y.-C., Prusoff, W.H., 1973. Relationship between the inhibition constant (Kᵢ) and the concentration of inhibitor which causes 50 percent inhibition (IC₅₀) of an enzymatic reaction. Biochem. Pharmacol. 22, 3099–3108. http://dx.doi.org/10.1016/0006-2952(73)90196-2.

Christmas, D.M., Potokar, J.P., Davies, S.J.C., 2011. A biological pathway linking inflammation and depression: activation of indoleamine 2,3-dioxygenase. Neuropsychiatr. Dis. Treat. 7, 431–439. http://dx.doi.org/10.2147/NDT.S17573.

Daniel, W., Adamus, A., Melzacka, M., Szymura, J., Vetulani, J., 1981. Cerebral pharmacokinetics of imipramine in rats after single and multiple dosages. Naunyn. Schmiedebergs. Arch. Pharmacol. 317, 209–213. http://dx.doi.org/10.1007/BF00503818.

Davies, A.R.L., Hardick, D.J., Blagbrough, I.S., Potter, B.V.L., Wolstenholme, A.J., Wonnacott, S., 1999. Characterisation of the binding of [³H]methyllycaconitine: a new radioligand for labelling α7-type neuronal nicotinic acetylcholine receptors. Neuropeptides (Oxford, United Kingdom) 38, 679–690. http://dx.doi.org/10.1016/S0028-3908(98)00221-4.

Elgoyhen, A.B., Katz, E., 2012. The efferent medial olivocochlear-hair cell synapse. J.

Physiol. Paris 106, 47–56. http://dx.doi.org/10.1016/j.jphysparis.2011.06.001.

Elgoyhen, A.B., Vetter, D.E., Katz, E., Rothlin, C.V., Heinemann, S.F., Boulter, J., 2001. α10: a determinant of nicotinic cholinergic receptor function in mammalian vestibular and cochlear mechanosensory hair cells. Proc. Natl. Acad. Sci. U. S. A. 98, 3501–3506. http://dx.doi.org/10.1073/pnas.051622798.

Feuerbach, D., Lingenhöhl, K., Dobbins, P., Mosbacher, J., Corbett, N., Nozulak, J., Hoyer, D., 2005. Coupling of human nicotinic acetylcholine receptors α7 to calcium channels in GH3 cells. Neuropharmacology 48, 215–227. http://dx.doi.org/10.1016/j.neuropharm.2004.10.003.

Goutman, J.D., Elgoyhen, A.B., Gómez-Casati, M.E., 2015. Cochlear hair cells: the sound-sensing machines. FEBS Lett. 589, 3354–3361. http://dx.doi.org/10.1016/j.febslet.2015.08.030.

Grando, S.A., 2006. Cholinergic control of epidermal cohesion. Exp. Dermatol. 15, 265–282. http://dx.doi.org/10.1111/j.0906-6705.2006.00410.x.

Gumilar, F., Arias, H.R., Spitzmaul, G., Bouzat, C., 2003. Molecular mechanisms of inhibition of nicotinic acetylcholine receptors by tricyclic antidepressants. Neuropharmacology 45, 964–976. http://dx.doi.org/10.1016/S0028-3908(03)00247-8.

Kalkman, H.O., Feuerbach, D., 2016. Modulatory effects of α7 nAChRs on the immune system and its relevance for CNS disorders. Cell. Mol. Life Sci. 73, 2511–2530. http://dx.doi.org/10.1007/s00018-016-2175-4.

Kumar, P., Meizel, S., 2005. Nicotinic acetylcholine receptor subunits and associated proteins in human sperm. J. Biol. Chem. 280, 25928–25935.

Liu, Q., Huang, Y., Shen, J., Steffensen, S., Wu, J., 2012. Functional α7β2 nicotinic acetylcholine receptors expressed in hippocampal interneurons exhibit high sensitivity to pathological level of amyloid β peptides. BMC Neurosci. 13, 155. http://dx.doi.org/10.1186/1471-2202-13-155.

López-Valdés, H.E., García-Colunga, J., 2001. Antagonism of nicotinic acetylcholine receptors by inhibitors of monoamine uptake. Mol. Psychiatry 6, 511–519. http://dx.doi.org/10.1038/sj.mp.4000885.

López-Valdés, H.E., García-Colunga, J., Miledi, R., 2002. Effects of clomipramine on neuronal nicotinic acetylcholine receptors. Eur. J. Pharmacol. 444, 13–19. http://dx.doi.org/10.1016/S0014-2999(02)01556-X.

Lykhmus, O., Voytenko, L., Lips, K.S., Bergen, I., Krasteva-Christ, G., Vetter, D.E., Kummer, W., Skok, M., 2017. Nicotinic acetylcholine receptor α9 and α10 subunits are expressed in the brain of mice. Front. Cell. Neurosci. 11 article282.

McIntosh, J.M., Absalom, N., Chebib, M., Elgoyhen, A.B., Vincler, M., 2009. α9 nicotinic acetylcholine receptors and the treatment of pain. Biochem. Pharmacol. 78, 693–702. http://dx.doi.org/10.1016/j.bcp.2009.05.020.

Mineur, Y.S., Picciotto, M.R., 2010. Nicotine receptors and depression: revisiting and revising the cholinergic hypothesis. Trends Pharmacol. Sci. 31, 580–586. http://dx.doi.org/10.1016/j.tips.2010.09.004.

Mizoguchi, H., Yuzurihara, M., Ishige, A., Sasaki, H., Tabira, T., 2001. Effect of chronic stress on cholinergic transmission in rat hippocampus. Brain Res. 915, 108–111. http://dx.doi.org/10.1016/S0006-8993(01)02834-7.

Mohammadi, S.A., Burton, T.J., Christie, M.J., 2017. α9-nAChR knockout mice exhibit dysregulation of stress responses, affect and reward-related behaviour. Behav. Brain Res. 328, 105–114. http://dx.doi.org/10.1016/j.bbr.2017.04.005.

Moore, M.A., McCarthy, M.P., 1995. Snake venom toxins, unlike smaller antagonists, appear to stabilize a resting state conformation of the nicotinic acetylcholine receptor. BBA - Biomembr. 1235, 336–342. http://dx.doi.org/10.1016/0005-2736(95)80022-8.

Morales-Perez, C.L., Noviello, C.M., Hibbs, R.E., 2016. X-ray structure of the human α4β2 nicotinic receptor. Nature 538, 411–415. http://dx.doi.org/10.1038/nature19785.

Morley, B.J., Whiteaker, P., Elgoyhen, A.B., 2018. Front. Cell. Neurosci. http://dx.doi.org/10.3389/fncel.2018.00104. in press.

Peng, H., Ferris, R.L., Matthews, T., Hiel, H., Lopez-Albaitero, A., Lustig, L.R., 2004. Characterization of the human nicotinic acetylcholine receptor subunit alpha (α) 9 (CHRNA9) and alpha (α) 10 (CHRNA10) in lymphocytes. Life Sci. 76, 263–280.

Ramirez, K., Sheridan, J.F., 2016. Antidepressant imipramine diminishes stress-induced inflammation in the periphery and central nervous system and related anxiety- and depressive- like behaviors. Brain Behav. Immun. 57, 293–303. http://dx.doi.org/10.1016/j.bbi.2016.05.008.

Romero, H.K., Christensen, S.B., Di Cesare Mannelli, L., Gajewiak, J., Ramachandra, R., Elmslie, K.S., Vetter, D.E., Ghelardini, C., Iadonato, S.P., Mercado, J., Olivera, B.M., McIntosh, J.M., 2017. Inhibition of α9α10 nicotinic acetylcholine receptors prevents chemotherapy-induced neuropathic pain. Proc. Natl. Acad. Sci. U. S. A. 114, E1825–E1832. http://dx.doi.org/10.1073/pnas.1621433114.

Sansone, R.A., Sansone, L.A., 2008. Pain, pain, go away: antidepressants and pain management. Psychiatry (Edgmont) 5, 16–19.

Shytle, R.D., Silver, A.A., Lukas, R.J., Newman, M.B., Sheehan, D.V., Sanberg, P.R., 2002. Nicotinic acetylcholine receptors as targets for antidepressants. Mol. Psychiatry 7, 525–535.

St-Pierre, S., Jiang, W., Roy, P., Champigny, C., LeBlanc, E., Morley, B.J., Hao, J., Simard, A.R., 2016. Nicotinic acetylcholine receptors modulate bone marrow-derived pro-inflammatory monocyte production and survival. PLoS One 11, e0150230. http://dx.doi.org/10.1371/journal.pone.0150230.

Tirado-Rives, J., Jorgensen, W.L., 2006. Contribution of conformer focusing to the uncertainty in predicting free energies for protein−ligand binding. J. Med. Chem. 49, 5880–5884. http://dx.doi.org/10.1021/jm060763i.

Vázquez-Gómez, E., Arias, H.R., Feuerbach, D., Miranda-Morales, M., Mihailescu, S., Targowska-Duda, K.M., Jozwiak, K., García-Colunga, J., 2014. Bupropion-induced inhibition of α7 nicotinic acetylcholine receptors expressed in heterologous cells and neurons from dorsal raphe nucleus and hippocampus. Eur. J. Pharmacol. 740, 103–111. http://dx.doi.org/10.1016/j.ejphar.2014.06.059.

Wallace, T.L., Porter, R.H.P., 2011. Targeting the nicotinic α7 acetylcholine receptor to enhance cognition in disease. Biochem. Pharmacol. 82, 891–903.

Weiss, J.N., 1997. The Hill equation revisited: uses and misuses. FASEB J. 11, 835–841.